SANDIA REPORT
SAND2017-10330
Unlimited Release
Printed September 2017

Impinging Water Droplets on Inclined Glass Surfaces

Kenneth M. Armijo, Blake Lance, and Clifford K. Ho

Prepared by
Sandia National Laboratories
Albuquerque, New Mexico 87185 and Livermore, California 94550

Sandia National Laboratories is a multimission laboratory managed and operated by National Technology and Engineering Solutions of Sandia, LLC, a wholly owned subsidiary of Honeywell International, Inc., for the U.S. Department of Energy's National Nuclear Security Administration under contract DE-NA0003525.

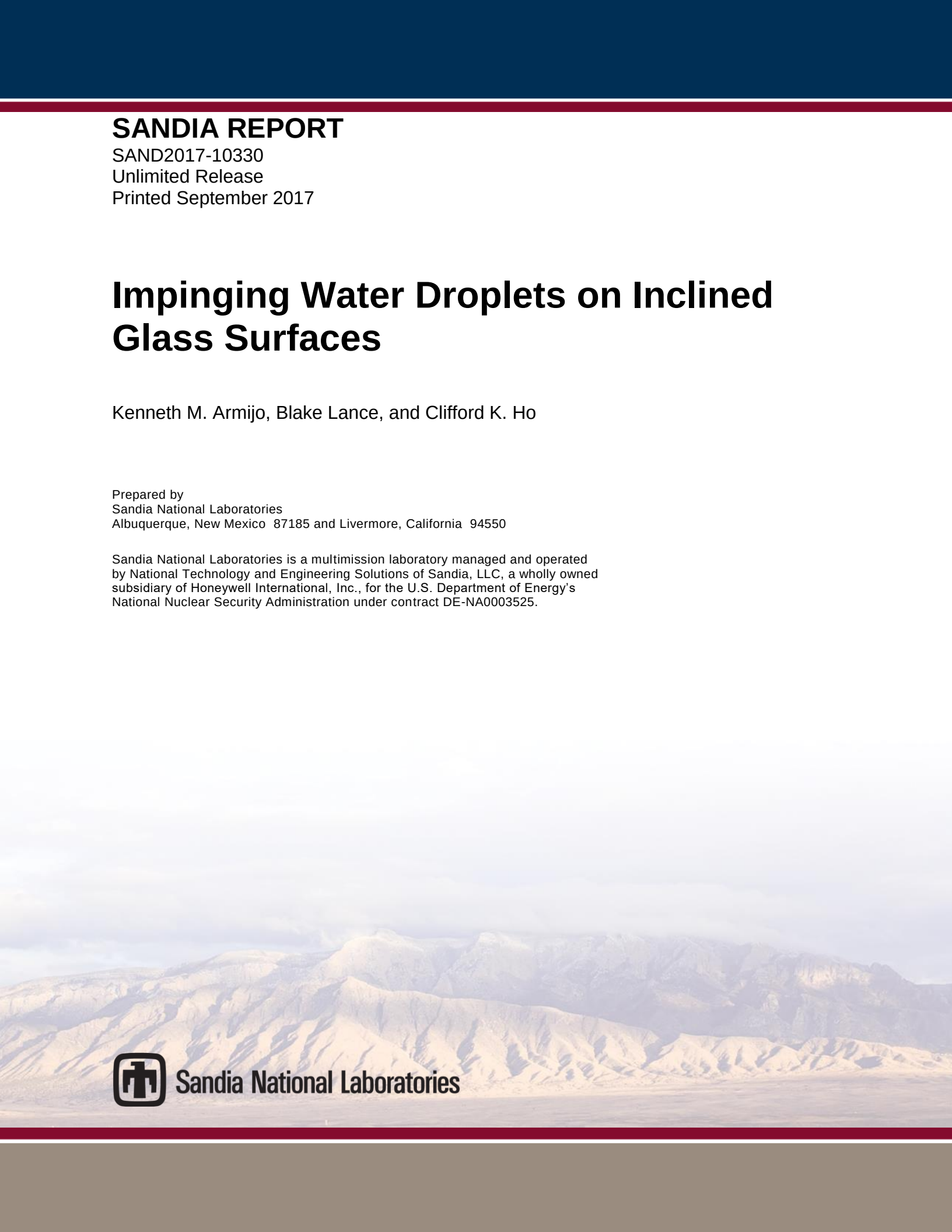

Issued by Sandia National Laboratories, operated for the United States Department of Energy by National Technology and Engineering Solutions of Sandia, LLC.

Available to DOE and DOE contractors from
U.S. Department of Energy
Office of Scientific and Technical Information
P.O. Box 62
Oak Ridge, TN 37831

Telephone: (865) 576-8401
Facsimile: (865) 576-5728
E-Mail: reports@osti.gov
Online ordering: http://www.osti.gov/scitech

Available to the public from
U.S. Department of Commerce
National Technical Information Service
5301 Shawnee Rd
Alexandria, VA 22312

Telephone: (800) 553-6847
Facsimile: (703) 605-6900
E-Mail: orders@ntis.gov
Online order: http://www.ntis.gov/search

SAND2017-10330
Printed September 2017
Unlimited Release

Impinging Water Droplets on Inclined Glass Surfaces

Kenneth M. Armijo,[1] Blake Lance,[2] and Clifford K. Ho[1]
[1]Org. 08823 Concentrating Solar Technologies
[2]Org. 08841 Advanced Nuclear Concepts
Sandia National Laboratories
P. O. Box 5800
Albuquerque, New Mexico 87185-1127

Abstract

Multiphase computational models and tests of falling water droplets on inclined glass surfaces were developed to investigate the physics of impingement and potential of these droplets to self-clean glass surfaces for photovoltaic modules and heliostats. A multiphase volume-of-fluid model was developed in ANSYS Fluent to simulate the impinging droplets. The simulations considered different droplet sizes (1 mm and 3 mm), tilt angles (0°, 10°, and 45°), droplet velocities (1 m/s and 3 m/s), and wetting characteristics (wetting=47° contact angle and non-wetting = 93° contact angle). Results showed that the spread factor (maximum droplet diameter during impact divided by the initial droplet diameter) decreased with increasing inclination angle due to the reduced normal force on the surface. The hydrophilic surface yielded greater spread factors than the hydrophobic surface in all cases. With regard to impact forces, the greater surface tilt angles yielded lower normal forces, but higher shear forces. Experiments showed that the experimentally observed spread factor (maximum droplet diameter during impact divided by the initial droplet diameter) was significantly larger than the simulated spread factor. Observed spread factors were on the order of 5 – 6 for droplet velocities of ~3 m/s, whereas the simulated spread factors were on the order of 2. Droplets were observed to be mobile following impact only for the cases with 45° tilt angle, which matched the simulations. An interesting phenomenon that was observed was that shortly after being released from the nozzle, the water droplet oscillated (like a trampoline) due to the "snapback" caused by the surface tension of the water droplet being released from the nozzle. This oscillation impacted the velocity immediately after the release. Future work should evaluate the impact of parameters such as tilt angle and surface wettability on the impact of particle/soiling uptake and removal to investigate ways that photovoltaic modules and heliostats can be designed to maximize self-cleaning.

ACKNOWLEDGMENTS

This work was funded by Sandia's Laboratory Directed Research & Development program (proposal #17-1073, project #206818, "Physics of Impinging Water Droplets on Inclined Glass Surfaces"). Sandia National Laboratories is a multimission laboratory managed and operated by National Technology and Engineering Solutions of Sandia, LLC., a wholly owned subsidiary of Honeywell International, Inc., for the U.S. Department of Energy's National Nuclear Security Administration under contract DE-NA0003525.

TABLE OF CONTENTS

FIGURES

TABLES

1. INTRODUCTION

1.1. Background and Problem Statement

Impinging water droplets on inclined glass surfaces has significant relevance for self-cleaning of photovoltaic (PV) modules and mirrors for solar energy technologies. To date, most research on self-cleaning of glass surfaces has focused on the development of superhydrophobic or superhydrophilic coatings to either mitigate water adhesion and soiling or to enhance the spreading and movement of rainwater to enhance cleaning, respectively. The actual physics of impinging and sliding/rolling water droplets on inclined glass surfaces relevant to removal of particulates has received relatively little attention. This work will develop multi-phase models of impinging and propagating water droplets as a function of impact velocity, droplet size, inclination angle, and thermophysical properties of the droplet (e.g., density and viscosity, which can be impacted by environmental parameters such as temperature and atmospheric composition). The impact, splatter (spread ratio), and subsequent gravity-driven motion of the droplet(s) will be simulated. Factors that impact particulate uptake and removal such as surface tension, particle size/density, and fluid dynamics within the droplet will be evaluated.

Developing an improved understanding of water droplet dynamics and particle absorption can improve methods for self-cleaning of PV modules and mirrors, which will increase overall performance and reduce levelized costs of these systems. This, in turn, can lead to greater penetration of renewables with increased reliability and sustainability of our energy infrastructure – primary goals for Sandia's and DOE's missions.

1.2. Objectives

The objective of this work is to develop physics-based, multi-phase models to simulate impingement and propagation of falling water droplets on inclined glass surfaces. The models will include physical-chemical properties of the water droplet (size, density, viscosity), glass surface (texturing or chemical treatment that may impact the surface tension of water), and particles (hydrophobicity, size, density). Computational fluid dynamics models employing volume-of-fluid methods to simulate free-surface flows of immiscible fluids (e.g., water/air) will be used to simulate impinging droplets on inclined surfaces. The resulting spread ratio, defined as the ratio of the resulting contact area of the splattered satellite droplets to the original area of the impinging droplet) will be determined as a function of droplet velocity, size, density, and surface properties. Subsequent propagation of the water droplet along the glass surface will also be simulated as a function of tilt angle and surface tension. Another objective is to design and perform experiments to visualize the impinging droplets on flat and inclined surfaces as a function of tilt angle, droplet velocity, and contact angle (wetting vs. non-wetting surface). Finally, a thorough literature review of past research regarding this topic is presented.

1.3. Previous Research

Solar energy systems, such as photovoltaic (PV) modules and concentrating solar power (CSP) heliostats exposed to hazy environments see an accumulation of dust, pollen and ash on their front glass surface reducing transmittance, facilitating a significant temporary performance loss, of up to 32% [1]. Self-cleaning surfaces have been previously investigated, with particular attention made to superhydrophobic surfaces (SHSs) where dust particles can be easily removed by water droplet impact, with subsequent spreading and rolling motion to further remove surface particulate

matter. Although there are numerous ways to clean glass surfaces, such as sandblasting and water spraying, these cleaning methods can be abrasive and damage surfaces which can facilitate further smudging and soiling. Additionally, cleaning can be intensive work, with large costs and massive use of chemical cleaning agents that can cause environmental problems [2]. Modified glass surfaces, that contain superhydrophobic surfaces (SHSs), having water contact angles greater than 150° and sliding angles smaller than 10°, are able to achieve self-cleaning by the "lotus effect" [3] with surface energies that can contribute to impingement forces capable of lifting dust during droplet impact. Studies by Furstner [4] and Quan et al. [3] investigated self-cleaning properties of three superhydrophobic surfaces where the authors determined that water droplets with some amount of kinetic impact energy, or impact pressure, were able to clean these surfaces perfectly. However, Quan [3] explained that in reality, superhydrophobic surfaces are less durable, where ordinary surfaces are more common and may still have some level of self-cleaning abilities under droplet impingement conditions. Quan et al. also noted that there is still a gap in the literature pertaining to published studies devoted to the effects of surface wettability and dust types on self-cleaning [3], which is of great importance to the successful realization of self-cleaning with hydrophobic surfaces in solar energy applications devoted to PV and CSP. Additionally, to date, although previous investigations have assessed applications of surfactants for soiling removal, reliability issues have persisted, where few investigators have also explored the potential removal of ash, pollen and varying compositions of soil sediment, which also have impacts on spectral absorption [5] on PV glass surfaces.

Phenomological liquid surface interactions for droplet impact and spreading has received much attention for a variety of technical applications such as thin film coating, pesticide application, spray painting, spray combustion, spray cooling of hot surfaces, deposition of solder bumps on printed circuit boards and inkjet printing [6-8]. Overall, two conditions for self-cleaning have been expounded upon in the literature: 1. Impact and lifting of dust particles by droplets, and 2. Spreading/rolling motion of droplets along surfaces at respective inclinations. When a liquid droplet contacts a wettable surface, the liquid spreads over the solid to minimize the total surface energy [9]. For water, which can be considered a low viscous fluid, a power law of the drop spreading can be observed during development of varying parameters such as gravity, density, surface tension, inertia, volume and viscosity. For many investigators [6,10,11] spread factor is used to characterized impact and spreading with a normalized spread factor parameter, $\xi(t)$, which is the ratio of droplet spread diameter on a surface, d(t), to the initial droplet diameter just before impact, d_0. For a droplet diameter of approximately 2 mm, Pasandideh-Fard et al. [11] developed an analytical energy conservation formulation, Eqn. (1) to characterize the maximum spread factor parameter as a function of Weber and Reynolds numbers to account for inertial and viscous effects:

$$\xi_{max} = \frac{d_{max}}{d_0} = \sqrt{\frac{We+12}{3(1-cos\theta)+4\left(\frac{We}{\sqrt{Re}}\right)}} \tag{1}$$

where We, Re and θ are respectively the Weber number, Reynolds number and contact angle. Subsequently, the transient effects for the spread factor as a function of time provides the maximum spread factor, d_{max}, [13]. As droplets increase in size, they become dominated by gravity effects [12], where the diameter of spreading can be characterized by Lopez's law by a $1/8^{th}$ power law [14,15]. Kavehpour further demonstrated, that as the radius grows larger beyond the capillary length, the droplet morphology changes to a more compressed shape of constant thickness, curved

only at the rim, where gravity forces dominate, leading to n = 1/7 [16,17]. Bonn et al. [18] elaborated that this extremely slow dynamics phenomena emerges from a balance between surface tension and viscous forces close to the contact line. Here, several empirical models have previously investigated the maximization of the spread diameter controlled through the use of solidification, uptake of liquid into a porous substrate, or surface roughness holding the liquid in the area of maximum spread [19].

Hu et al. [13] further investigated droplet impingement with subsequent spreading using high-speed photography where resultant observations at approximately 1 to 100 μs after the drop contacted the surface found that the inertia of the moving drop resisted capillary forces that drive high speed spreading (at ~1 m/s) [2]. The spreading dynamics were also found to follow a power law with $d = 2Kt^{0.5}$, which was independent of surface wettability, also verified by [20,21]. Here, K was the spreading coefficient where its utility is used in common practice to distinguish a droplet that splashes and one that does not, where K_{crit} is defined as the threshold of splash [22]. For time scales at approximately 0.1 to 10 ms (with a drop spreading velocity of approximately 0.1 m/s), Hu et al. found that spreading was still dominated by inertia [13]. Beyond this time scale, the authors explained that the surface wettability begins to strongly influence the growth of the spreading radius that grows with time according to a separate power law $d = 2K't^{\alpha}$, where K' is a spreading coefficient for larger time scales, and α is only dependent on the equilibrium contact angle θ_{eq} [12]. Another approach to droplet impingement prediction modelling has been through the employment of a droplet splash parameter, which has been used predict the presence or absence of splash [11,23], where few studies exist quantifying the mass of splash expected from a drop [22]. In a study by Brown et al. [24] the splash parameter, %Splash Eqn. (2), was presented with respect to the mass of glycerin ejected from the impact region as a function of We.

$$\%Splash = \frac{100We}{We+10^6} \tag{2}$$

A review of droplet impact models by Cossali et al. indicated many shortcomings for empirical droplet impact models [25] where most were found only appropriate in limited regimes of velocity and drop diameter. Here, the authors indicated that much of the fidelity that might be expected from realistic phenomena were not well reproduced in the models, where many of the models studied resulted in widely divergent predictions. These models also did not provide details for the directional mass distribution of the splash, or the fraction of mass remaining on the surface following impact [26]. Additionally, although surface perpendicular droplet impacts have been well studied, less attention has been given to impact geometries on angled surfaces. In a review by Yarin [27] the author concluded that the consequences of oblique impacts on dry surfaces are still insufficiently studied and understood, where subsequent oblique surface studies still only focused on small Weber number impacts without splashing [28,29]. Due to added complexity with oblique geometries, studies are normally limited to that which can be extracted from photometric analysis [22]. However, energetic impacts have been found to facilitate instabilities during the spreading of droplets or fingers at higher velocities [30], which can also be quite dependent on surface angle as well [22]. Jespen et al. [31] performed droplet impact studies as a function of We, impact angles ranging from 45-90°, droplet diameters of 0.2 to 10 cm and impact velocities from 1 to 20 m/s, where the authors demonstrated that impact angle affects the total number of fingers as well as the number of fingers spreading uphill, downhill or sideways from the impact point. They also found that algebraic drop spread models underpredicted the final spread by a small amount (5-35%).

Variation of the ambient pressure was also found to affect fingering formation, where the total number of fingers decreased as impact angle was adjusted from 90 to 45 degrees [31].

The impact force or pressure of a water droplet impingement with surfaces has had much analytical study [32-34] where early attempts by Cooks et al. [10] saw expressions developed for the impact pressure generated by droplet collision on solid surfaces, where the water-hammer expression developed for pressure was considered sufficient [41] to characterize the erosion of steam turbine blades. On the basis of one-dimensional analysis incorporated with the variable shock wave velocity, Heymann [35] extended Cooks water-hammer relation by further developing a two-dimensional approximation, valid for the "initial" phase of impact, just prior to spreading. The authors results suggested the maximum instantaneous impact pressure for water was approximately 3 times that of the water-hammer pressure for the case of impact Mach number ranging from 0.03 to 0.35. However, his work did not provide information about the pressure distribution within the instantaneous contact area. However, more modern numerical simulations [36,37] that have investigated liquid-solid impact forces, pressure/stress distributions on solid plates during droplet-solid collision have been performed, where research by Adler [36] investigated the impact process of a 2-mm diameter water droplet with a velocity of 305 m/s on a zinc surface. Here, and the general behavior of a water droplet impact on deformable surfaces appeared to be adequately represented. Keegen et al. [38] developed an explicit dynamics software package to model a rain droplet colliding with an Epoxy resin plate at speeds ranging from 40 m/s to 140 m/s, where the resultant impact forces and pressures were consistent with the data obtained from standard analytical relations. Li et al. [39] and Zhou et al. [40] proposed to couple the interaction between the liquid droplet and the elastic solid surface by solving the wave equation for liquid droplets and the Lame equation for the solid elastodynamics. The investigators determined that although the nonlinear wave equation for the droplet is only valid for the initial stage of impact just prior to spreading, the impact duration was long enough to identify the maximum impact pressure. Their results showed that for modelled droplets at an impact speed of 100 m/s, the maximum liquid pressure at the contact edge reached values of approximately 3 times that of water hammer pressure at the moment when the shock wave was going to break away from the liquid. These results further corresponded to the results of Heymann [35]. However, this phenomena does not occur for lower speeds [41]. For a droplet impact speed of 10 m/s, Li et al. [41] concluded that the resultant pressure was close to the water hammer pressure, where no evidence of shock waves could be found in the droplet.

When a droplet impacts an inclined surface, its spreading motion determines the size of the area to be cleared, where its recoiling behavior determines the ability to remove particles. It can be found that only the water-air interface at the trailing edge of the droplet can pick up particles efficiently during the recoiling process. These particles then tend to move toward the center or to the front of the drop, which is driven by the velocity field inside the droplet as well as forces at the respective interfaces between liquid, gas and solid [3]. This work will investigate water droplet impingement and physicochemical hydrodynamic phenomena based on varying compositions and geometries with implications on soiling remediation for PV and CSP glass and laminated surfaces. Here 3D transient Volume of Fluid (VOF) parametric models will be developed using ANSYS Fluent® where parallel experimentation using high-speed photography will analyze the removal potential of rain droplet impacts, with subsequent liquid propagation. Velocity is known to increase the maximum extent of spreading to a limit where splashing occurs and small satellite droplets are ejected [47]. This work will also assess two initial droplet velocities to assess droplet impact,

spreading and the propagation of subsequent satellite droplets. Additionally, augmentation of surface tension properties can occur based on the addition of surfactants which can be used to increase the final wetted surface area of droplets and subsequent dust removal. This work will also include parametric evaluation of two contact angles, one that is hydrophilic and one that is hydrophobic. The general variation trend of the impact force we hypothesize is that it will increase sharply at first, and then begin to decrease slowly to zero, with oscillation observed.

2. MODELING

2.1. CFD Model Development

This investigation will characterize droplet impact and spreading with a normalized spread factor, defined as the ratio of the droplet spread diameter on the substrate surface to the initial droplet diameter prior to impact. Here, parametric analysis was performed based on measurement of droplet size (3 mm and 5.4 mm), impact velocity (1 m/s and 3 m/s), surface geometry (inclination angles of 0°, 10° and 45°) and wettability based on two measured hydrophilic (47°) and hydrophobic (93°) contact angles. To simulate the impact process of the droplet on a solid surface, the volume of fluid (VOF) method will be employed to track the free surface of the droplet such that with each cell nonlinear coupled differential equations representing fluid flow are integrated over the cell control volume [42]. The VOF approach will model fluid motion of two immiscible fluids where the single momentum equation is solved throughout the domain with the resulting velocity field shared among the phases, Eqn.(3):

$$\frac{\partial}{\partial t}(\rho\vec{v}) + \nabla\cdot(\rho\vec{v}\vec{v}) = -\nabla p + \nabla\cdot[\mu(\nabla\vec{v} + \nabla\vec{v}^{T})] + \rho\vec{g} + \vec{F} \tag{3}$$

In a VOF model, the conservation equations representing the fluid flow are derived with an assumption of continuum, which means that there are no abrupt changes in the fluid properties, where the resulting set of algebraic equations are then solved simultaneously to get the flow field in the domain [43]. For each additional phase that is added to the model, a separate volume fraction of the phase in the computational cell is added. In each control volume, the volume fractions of all phases sum to unity where the tracking of the interface(s) between the phases is accomplished by the solution of a continuity equation for the volume fraction of one (or more) of the phases. The physical properties of the mixture density ρ and laminar viscosity μ are expressed as functions of the phase properties and liquid volume fraction α, which is defined as the ratio of liquid fluid volume over the total fluid volume in a computational cell:

$$\rho = \rho_g(1-\alpha_l) + \rho_l\alpha_l \tag{4}$$
$$\mu = \mu_g(1-\alpha)_l + \mu_l\alpha_l \tag{5}$$

The VOF model was developed using ANSYS FLUENT® where the VOF approach is generally recommended for computing time-dependent solutions [43]. The computational model was broken up into two separate droplet and air domains as shown in Figure 1a. for a 3 mm droplet, where the ambient pressure and temperature was set at 1 atm and 25 °C. Although previous work [44] has shown that these two parameters can impact droplet impact and spreading, they were not varied

here. A three-dimensional approach was performed for the droplet impact process primarily to account for the non-symmetric domain conditions. Here, the computational domain was determined to be approximately 2.5 cm and 2.5 cm for the width and depth respectively, with a pressure-inlet condition on the top surface where the side boundaries were modelled as pressure outlet conditions. The droplets were all initially approximated to be spherical and centralized 2 mm above the solid surface, where the droplet domain was initialized with a patch to be liquid water and with a respective initial velocity. The surface was modelled as a non-slip wall condition. Grid independence, as well as the effects of the time step based on the Courant number, and the size of the computational domain were all investigated to make sure that the simulation was reliable and the mesh converged. The resultant mesh used for each of the modelled cases, as shown in Figure 1b, had refinement performed at the surface with a total cell count of approximately 300,000 cells, and a time step of $1x10^{-5}$ s. 700 internal iterations per time step were also imposed per simulation. The simulation for each time step was regarded as convergent when the residuals decreased below $1x10^{-4}$. Fluent solution options were also as follows: the PISO scheme for the pressure velocity coupling in the momentum equation; the second order upwind scheme for the convective terms in the equations of the momentum, volume fraction, turbulence kinetic energy, and turbulence dissipation rate; the second order implicit method for the transient formulation.

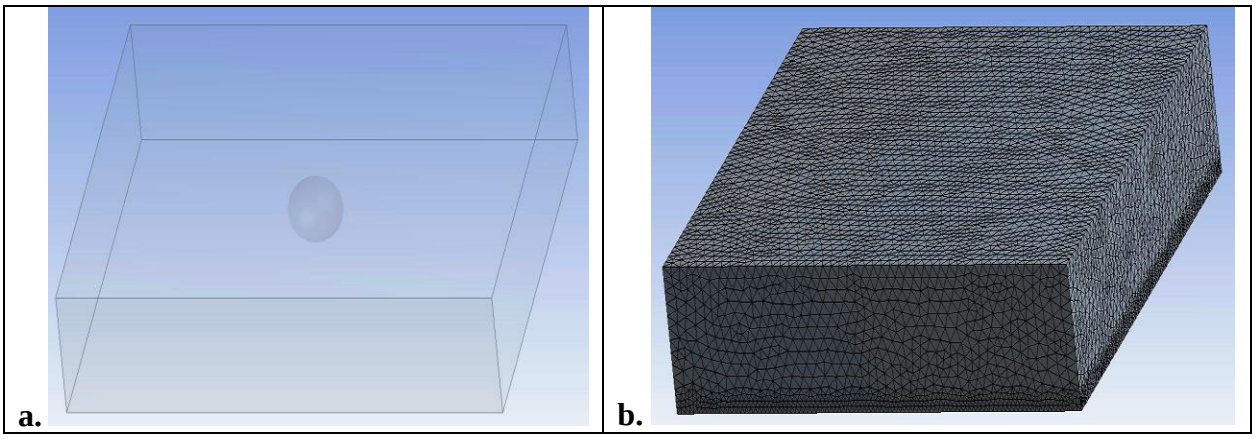

Figure 1. Computational model a. domain and boundary conditions of water droplet (red) within an air (blue) domain, and b. convergent mesh used within the simulation.

For this model, an explicit Runge-Kutta time integration scheme was employed for time discretization where ANSYS Fluent's standard finite-difference interpolation schemes for VOF were used (First Order Upwind, Second Order Upwind, CICSAM, Modified HRIC, and QUICK schemes) to obtain the face fluxes for all cells, including those near the interface. Turbulence model SST k-ω was selected from the two-equation viscous models, which has the advantage of lower computational demands. This is the most modern model of two-equation turbulence models available in ANSYS FLUENT® [43]. Model SST k-ω combines the robustness and accuracy of the k-ω model in areas close to the wall, whereas the k-ε model operates better in free flow. The SST k-ω model contains a modified turbulent viscosity formulation to account for transport effects of the principal turbulent shear stress [43].

For this analysis, the surface tension was specified based on values provided by NIST [45] with a value of 0.071 N/m based on an assumed ambient modelled system temperature of 25 °C. Surface tension arises as a result of attractive forces between molecules in the fluid to maintain equilibrium.

At the surface, the net force is radially inward, and the combined effect of the radial components of force across the entire spherical surface is to make the surface contract, thereby increasing the pressure on the concave side of the surface [43]. Therefore, in the regions where two fluids are separated, the surface tension acts to minimize free energy by decreasing the area of the interface. The surface tension model in ANSYS FLUENT® is the continuum surface force (CSF) model proposed by Brackbill et al. [46]. With this model, the addition of surface tension to the VOF calculation results in a source term in the momentum equation.

2.2. CFD Model Results

For this investigation several parameters were evaluated with respect to droplet impact and subsequent spreading. For this work only 3 mm diameter droplets have currently been analyzed with 3 m/s velocities imposed for 0°, 10° and 45° inclination angles. For the 45° inclination angle simulations, an additional 1 m/s imposed velocity was also evaluated for comparison. The 10° inclination angle was chosen based on experimental observation of droplets not sliding down the inclined surface after impingement. As shown in Figure 2 for a droplet impacting a 0° inclined surface at a speed of 3 m/s, the initial contact behavior at 1.3×10^{-3} s portrays an approximate symmetric jetting of fluid about the point of impact.

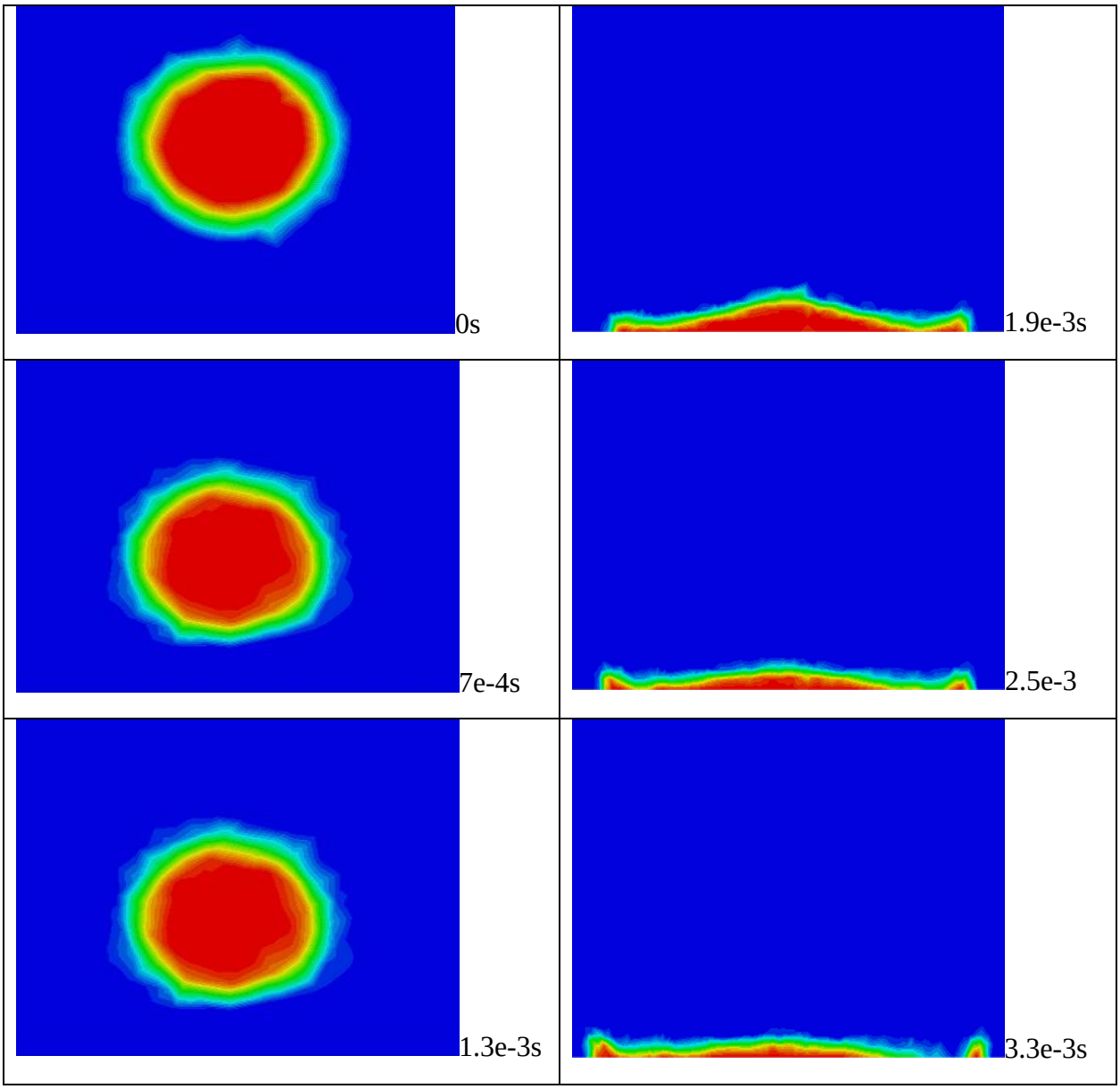

Figure 2. Time lapse profiles for a 3 mm droplet with a 3 m/s initial velocity, incident on a 0° inclination angled surface with a 47° contact angle.

As the droplet progresses across the surface the spread factor was calculated as shown in **Error! Reference source not found.**, where the largest values were found for the horizontal and lower inclination surfaces, which could be due to the lack of gravitational forces coalescing the bulk fluid together as it passes down a slope.

.

Table 1. Droplet spread factor for varying inclination angle, surface wettability and imposed velocity (all cases assume 3 mm droplet size and 3 m/s velocity except where noted).

Inclination Angle [°]	Hydrophilic Surface (47°)	Hydrophobic Surface (93°)
0	1.974	1.684
10	1.968	1.662
45	1.476	1.332
45 (1m/s)	3.621	2.457

For droplets with large levels of initial momentum, contact with the surface was found to spawn smaller satellite droplets that eventually broke away from the bulk fluid region as spreading continued. As shown in **Error! Reference source not found.**, the results suggest for droplets with a speed of 3 m/s that an increase of inclination angle to 10°, or increase contact angle produced the same number of satellite droplets as with a horizontal, hydrophilic surface. However, an increase in inclination to 45° did appear to slightly increase the number of satellite droplets for the hydrophilic surface, though a decrease was found for the hydrophobic surface.

Table 2. Satellite droplet formation after impact of a 3 mm droplet onto 0°, 10°, and 45° surfaces (all cases assume 3 mm droplet size and 3 m/s velocity except where noted).

Inclination Angle [°]	Hydrophilic Surface (47°)	Hydrophobic Surface (93°)
0	2.00	2.00
10	2.00	2.00
45	3.00	1.00
45 (1m/s)	0.00	0.00

After impact, the dislocation of satellite droplets became further pronounced as the respective bulk fluid regions spread across the surface (Figure 3). However, one should note that these illustrations are 2D projections from a 3D space, where further satellite droplets could also be present, where further analysis is still required to determine the total number created. Further simulations with droplets imposed with a lower velocity of 1 m/s along the 45° inclination angle found that the impact momentum was not great enough to dislocate these smaller droplets.

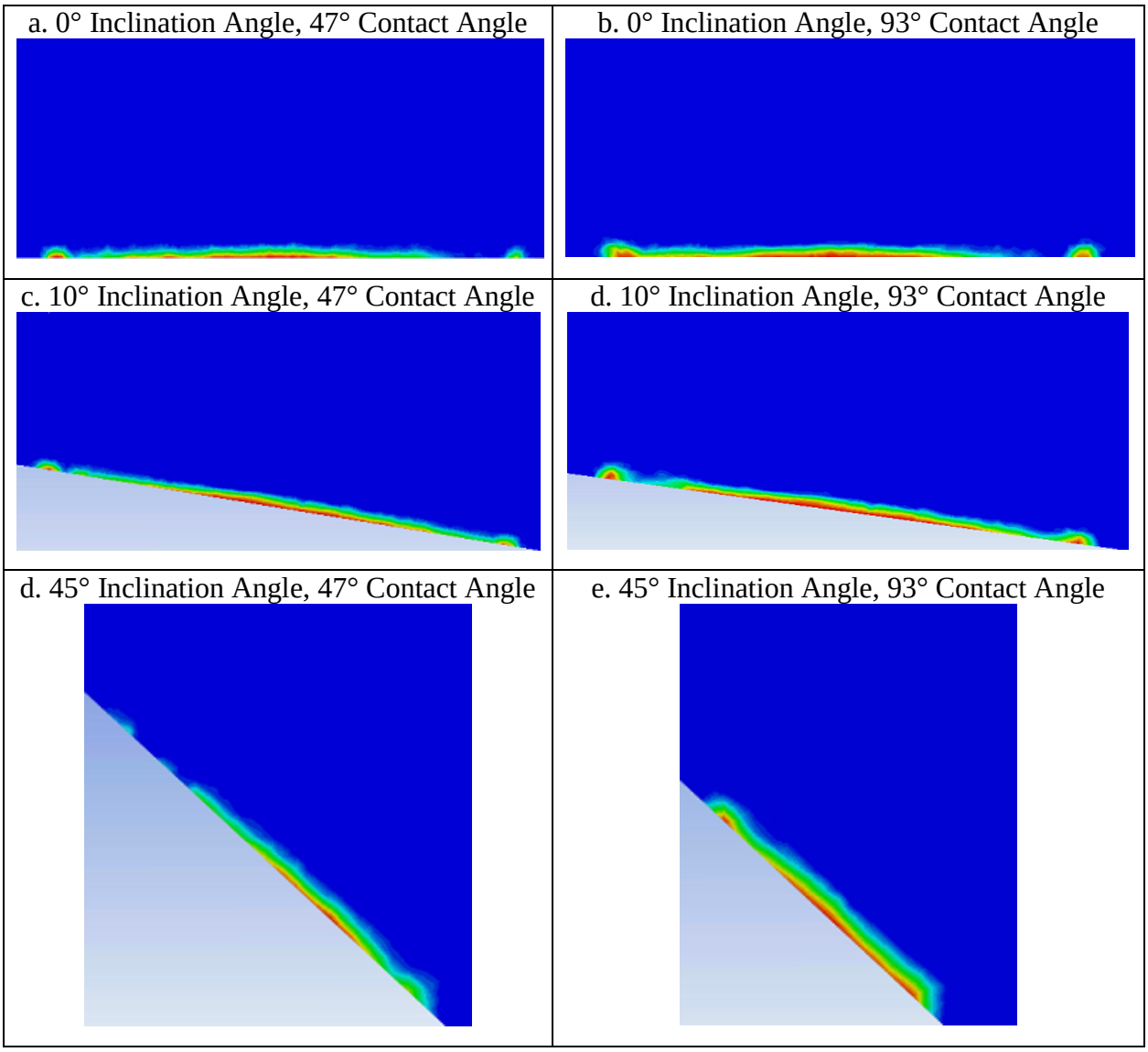

Figure 3. Parametric droplet impingement profiles along the gray solid surface, with an initial droplet velocity of 3 m/s, where blue and red represent volume fractions of 0 and 1 respectively.

Analysis was performed to investigate the static force produced by the droplet onto the surface over the early evolvement of droplet impact with subsequent spreading thereafter. As shown in Figure 4 larger impact forces were found for lower inclination angles overall, particularly for imposed velocities of 3 m/s from that of 1 m/s.

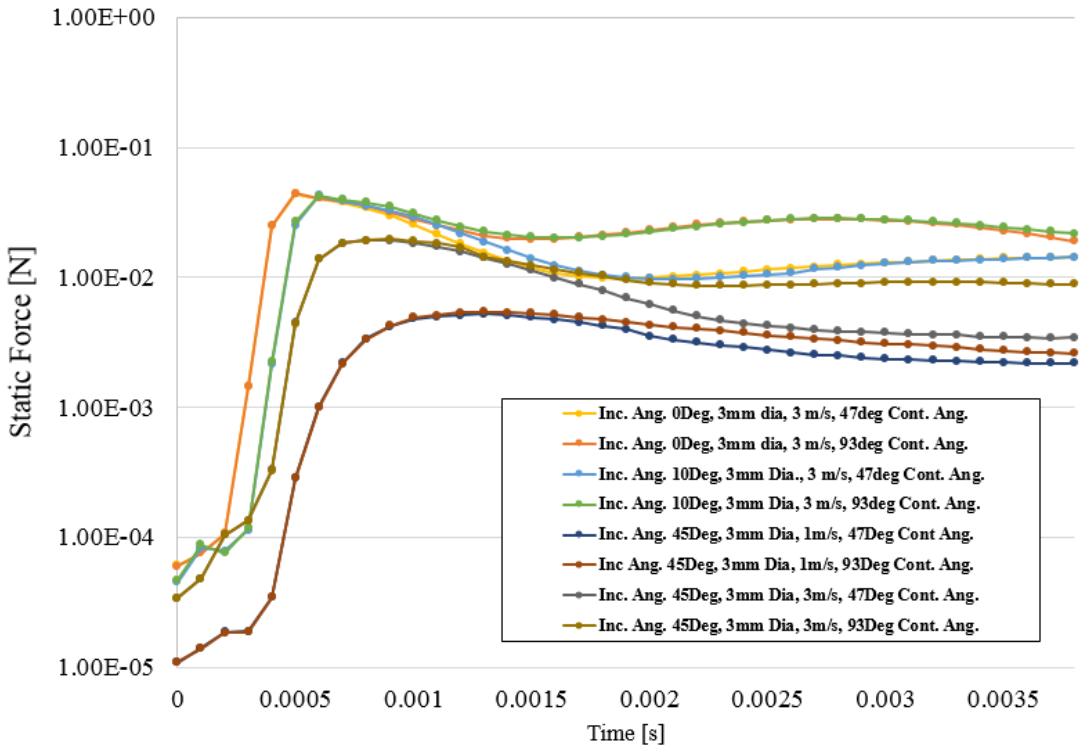

Figure 4. Liquid droplet static impact force temporal profile starting at impact t=0.

Further results of the static force assessment, **Error! Reference source not found.**, reveal the largest maximum values were executed with droplets impacting a horizontal surface, where an average force decrease of 56% was found as the surface inclination grew to 45°.

Table 3. Maximum static surface forces [N].

Inclination Angle [°]	Hydrophillic Surface (47°)	Hydrophobic Surface (93°)
0	4.39E-02	4.43E-02
10	4.27E-02	4.23E-02
45	1.93E-02	1.97E-02
45 (1m/s)	5.23E-03	5.46E-03

However, an analysis of surface forces directionally acting along the inclined surface, **Error! Reference source not found.**, revealed significantly higher forces for larger inclined surfaces than with horizontal or the 10° inclination angle.

Table 4. Maximum force along the inclined surface direction [N].

Inclination Angle [°]	Hydrophillic Surface (47°)	Hydrophobic Surface (93°)
0	1.56E-05	1.61E-05
10	6.57E-04	6.57E-04
45	9.42E-04	8.65E-04
45 (1m/s)	2.23E-04	6.26E-04

For all cases, the difference in hydrophobicity did not have an effect since the maximum forces were realized primarily during impact, however as spreading continued thereafter divergence became apparent as expected between all hydrophobic and hydrophilic cases as the droplets progressed across their respective surfaces.

3. EXPERIMENTS

3.1. Experimental Approach

Experiments were performed with water drops on both the hydrophilic and hydrophobic surfaces; with varying panel angles of 0, 10, and 45° from horizontal; and with nominal impact velocities of 1 and 3 m/s. Experimental case labeling used herein is provided in Table 5. The experimental results can provide great insight into the drop behavior as it releases, falls, impacts, and comes to rest. They can also be used for comparison with computational results in validation studies when the conditions are matched.

Table 5. Experimental test matrix of the twelve cases.

Case	Surface	Angle [°]	Impact Velocity [m/s]
1	Hydrophilic	0	~1
2*	Hydrophilic	0	~3
3	Hydrophilic	10	~1
4	Hydrophilic	10	~3
5	Hydrophilic	45	~1
6	Hydrophilic	45	~3
7	Hydrophobic	0	~1
8*	Hydrophobic	0	~3
9	Hydrophobic	10	~1
10	Hydrophobic	10	~3
11	Hydrophobic	45	~1
12	Hydrophobic	45	~3

*Note: these cases were performed in triplicate to test repeatability

Measurements of droplet parameters were made with a Phantom v9.1 high speed camera at 1000 frames/second at full camera resolution. Droplet position tracking as well as size and angle measurements were performed with Phantom Camera Control (PCC) software. The experimental setup with solar panel, high speed camera, and water dropper is shown in Figure 5.

Figure 5. Experimental setup with solar panel, high speed camera, and water dropper.

An example full-resolution camera image is shown in Figure 6 for Case 9 with the drop in its final position, the dropper at the top and the panel at the bottom. Note that the drop has shifted slightly from its impact location but not shed off the panel in this case. The solar panels themselves were included in the images and used for spatial calibration between length and pixels for each experiment since the solar cells have known dimensions.

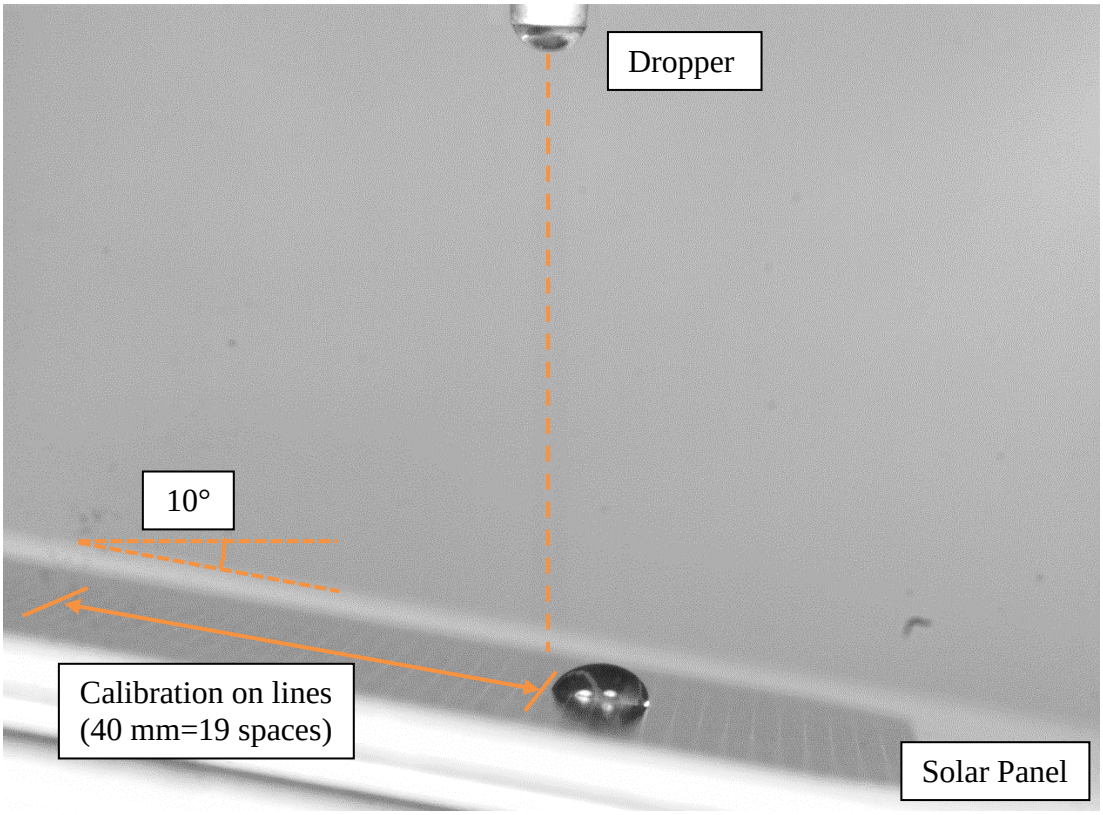

Figure 6. Example camera image for Case 9.

Several measured parameters are shown in three phases of Case 9 in Figure 7. The drop diameter D is measured during freefall when the shape is most spherical. The maximum diameter after impact D_{impact} is similarly measured. The contact angles can be identified in this image with the advancing/maximum angle, θ_{max}, greater than receding/minimum, θ_{min}, consistent with literature. Impact velocity V_i is measured as described in the next paragraph. The high speed recordings are used to also qualitatively record the number of satellite drops after impact (if any) $N_{satellite}$ and whether drops were mobile after impact (mobility).

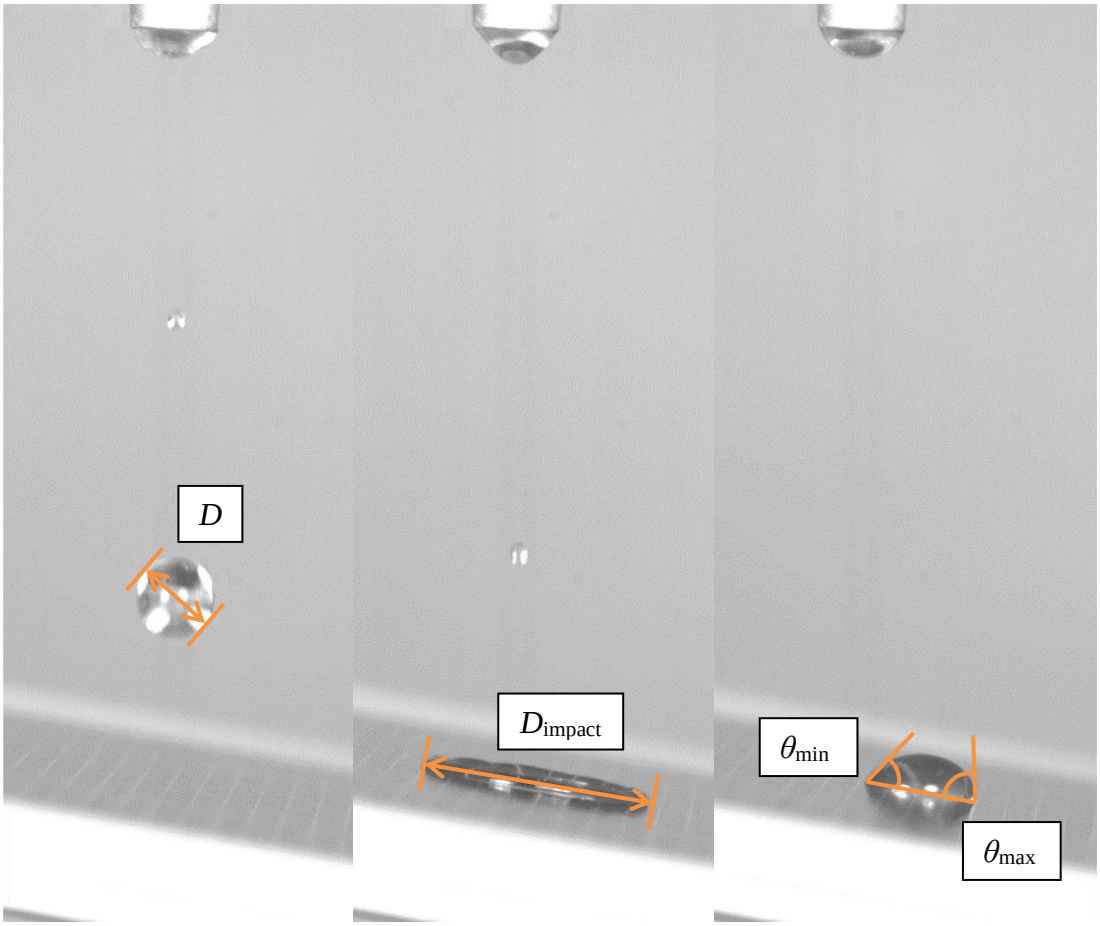

Figure 7. Several measurement parameter definitions.

Drop velocity was tracked in PCC software by identifying reflective features on the drop and determining displacement between frames. With the accurate timing inherent in high speed cameras, the velocity can be calculated by displacement over time using a second-order accurate central difference finite difference method. Figure 8 shows an example image showing the tracking feature and the window in which the feature should be tracked. Two spotlights were used to illuminate the experiment and caused distinct reflections on each drop that were used for tracking. The inner blue square contains this feature and the outer yellow rectangle is the area in which the search was performed, elongated in the vertical direction to better match the nearly-vertical falling motion. The vertical blue line is the tracked path of the feature and shows the vertical motion from the dropper to the panel.

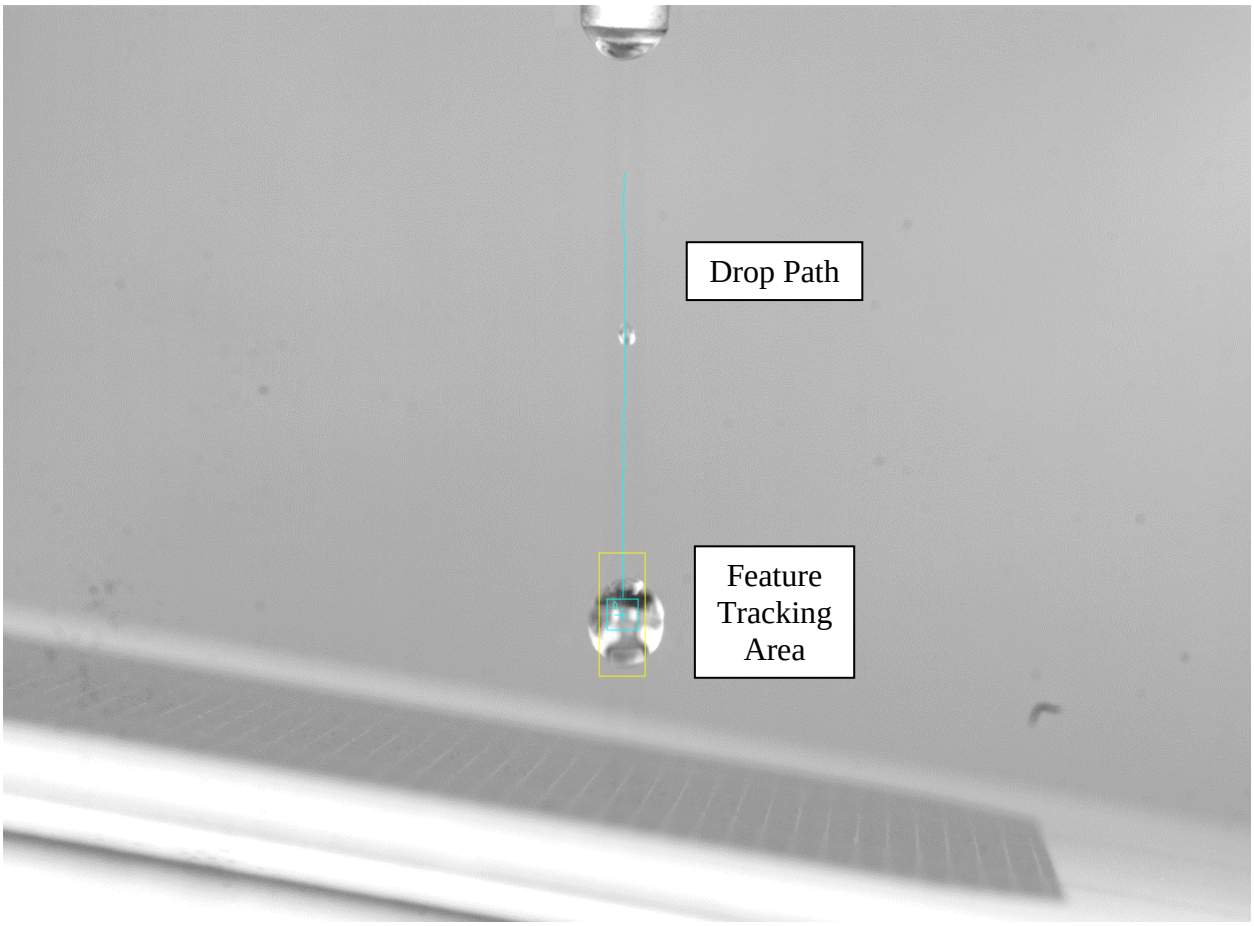

Figure 8. Drop feature tracking area and drop path.

3.2. Experimental Results

Even though experimental parameters varied conditions, each case had similar behavior that was observed. A time history of notable behavior for Case 9 is show in Figure 9 with labelling of 1—6. The phases are identified as

1. Droplet diameter measurement
2. Before impact
3. Initial impact
4. Progressed impact
5. Maximum impact diameter
6. Final

The final phase was used for the contact angle measurement when the drop was not mobile. Mobility was observed for the 45° cases for both surfaces and both impact velocities. Many cases had a small secondary drop that followed the first, but it did not have a significant influence on the final state.

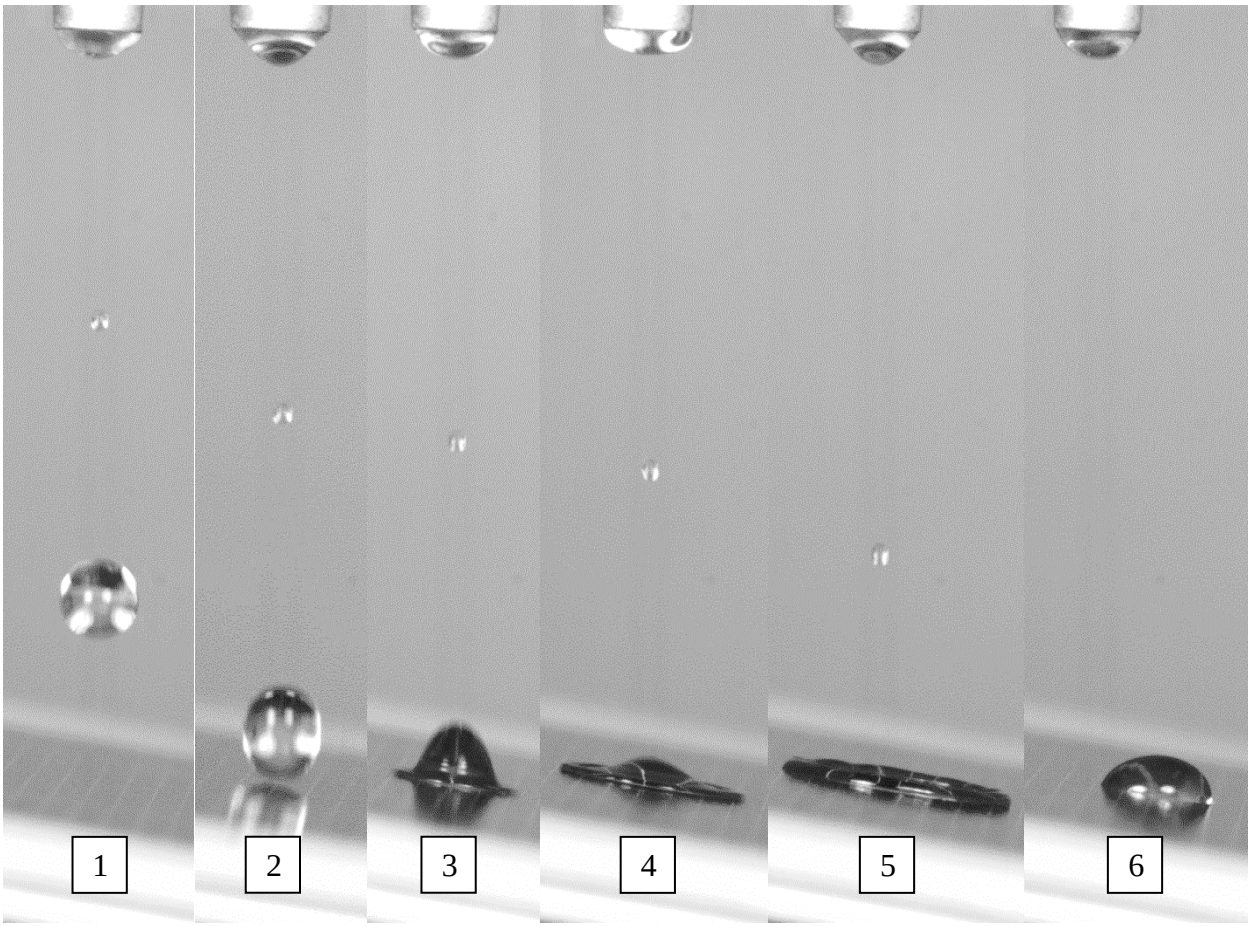

Figure 9. Time series of drop progression for Case 9.

The experimental results are summarized in Table 6 for all cases. There are several observations that can be made. The impact velocities were somewhat lower than the nominal 1 and 3 m/s, but they were measured and can be correlated to dependent variables. The average velocities were 0.909 and 2.83 m/s, respectively. The drop diameter was moderately consistent with an average of 5.39 mm. The maximum drop diameters after impact showed a large dependence on impact velocity with measurements of 16.3 mm and 28.1 mm, respectively, for the 1 and 3 m/s cases. Only Cases 6 and 12 had observed satellite drops resulting from the 45° angle and the higher velocity. Because satellite drops were observed for both hydrophilic and hydrophobic surfaces, it can be concluded that drop dynamics play a major role and not surface treatment for droplet formation. The high angle and velocity conditions likely caused an asymmetry of momentum that caused the formation. Mobility, or the shedding of drops after impact, was observed for all cases at the 45° angle and not at lower angles. There are likely two unique angles between 10 and 45° where each surface treatment will start to shed drops that could be a topic of further study. Contact angles had variability from side to side in a given test, even at 0°. This is likely from asymmetries in the drop shape upon impact. The difference in maximum and minimum angles is greater for greater inclination angle as expected. Contact angles for cases with mobility were not measured as the drops left the image area.

Table 6. Experimental results for all cases.

Case	Surface	*Angle* [°]	V_i [m/s]	D [mm]	D_{impact} [mm]	*Spread Factor*	$N_{satellite}$	Mobility [Y/N]	θ_{min} [°]	θ_{max} [°]
1	Hydrophilic	0	0.984	5.54	16.4	2.96	0	N	41.9	43.7
2*	Hydrophilic	0	2.82	5.32	27.1	5.09	0	N	25.4	23.1
3	Hydrophilic	10	0.862	5.43	16.4	3.02	0	N	34.7	50.3
4	Hydrophilic	10	2.82	5.52	27.9	5.05	0	N	9.0	44.1
5	Hydrophilic	45	0.992	5.64	15.9	2.82	0	Y	-	-
6	Hydrophilic	45	2.87	5.13	29.1	5.67	8	Y	-	-
7	Hydrophobic	0	0.947	5.21	16.3	3.13	0	N	63.0	74.9
8*	Hydrophobic	0	2.86	5.39	27.3	5.06	0	N	53.5	49.8
9	Hydrophobic	10	0.923	5.39	16.1	2.99	0	N	68.6	96.2
10	Hydrophobic	10	2.80	5.17	27.6	5.34	0	N	30.1	62.6
11	Hydrophobic	45	0.745	5.71	16.7	2.92	0	Y	-	-
12	Hydrophobic	45	2.83	5.52	29.7	5.38	9	Y	-	-

*Note: these cases were performed in triplicate and averaged

Two cases, 2 and 8, were repeated in triplicate for a measure of repeatability. They both had a panel angle of 0° and velocity around 3 m/s. The unique measurements are shown in Table 7 with the averages and standard deviations. With the exception of contact angles, the measured values are very repeatable with standard deviations of less than 2.1%. It is likely that the contact angles, with standard deviations up to 44%, have an independent parameter that was not consistent between cases. This could be drop shape upon impact, panel surface characteristics, or even secondary drop impingement. It is interesting to note that between repetitions the variability is high but for a given experiment θ_{min} and θ_{max} are more similar.

Table 7. Repeatability measurements. Note that parameters for all are 0° angle, $N_{satellite}$ = 0, Mobility = N.

Case	Surface	V_i [m/s]	D [mm]	D_{impact} [mm]	θ_{min} [°]	θ_{max} [°]
2-1	Hydrophilic	2.86	5.26	27.1	15.4	11.6
2-2	Hydrophilic	2.80	5.40	26.6	27.1	27.1
2-3	Hydrophilic	2.80	5.29	27.6	33.7	30.7
2-ave	Hydrophilic	2.82	5.32	27.1	25.4	23.1
2-std	Hydrophilic	0.035	0.075	0.485	9.25	10.1
8-1	Hydrophobic	2.85	5.38	27.2	45.0	45.9
8-2	Hydrophobic	2.88	5.51	27.2	52.7	46.1
8-3	Hydrophobic	2.84	5.29	27.4	63.0	57.3
8-ave	Hydrophobic	2.86	5.39	27.3	53.5	49.8
8-std	Hydrophobic	0.021	0.111	0.101	9.01	6.53

The behavior of the drop release can be analyzed for the 1 m/s cases where the dropper is included in the top of the image. The surface tension of water causes a delayed release and drop shape oscillations. In the initial stages of drop formation, the surface tension creates a web that holds

the top of the drop and causes elongation in the vertical direction as shown in Figure 10 for Case 3. The release causes a 'snapback' behavior where the elongated drop is then flattened by the rapid change in surface tension. This elongation-flattening behavior is observed several times within the same experiment before impact. The 3 m/s cases had a much higher drop height where these oscillations were damped out before the imaging field of view. In the rain application, these oscillations would not be present but could be an explanation for contact angle differences in the experiment. The release rate of water to form the drop was not controlled, so drop shapes could have been different at the time of impact.

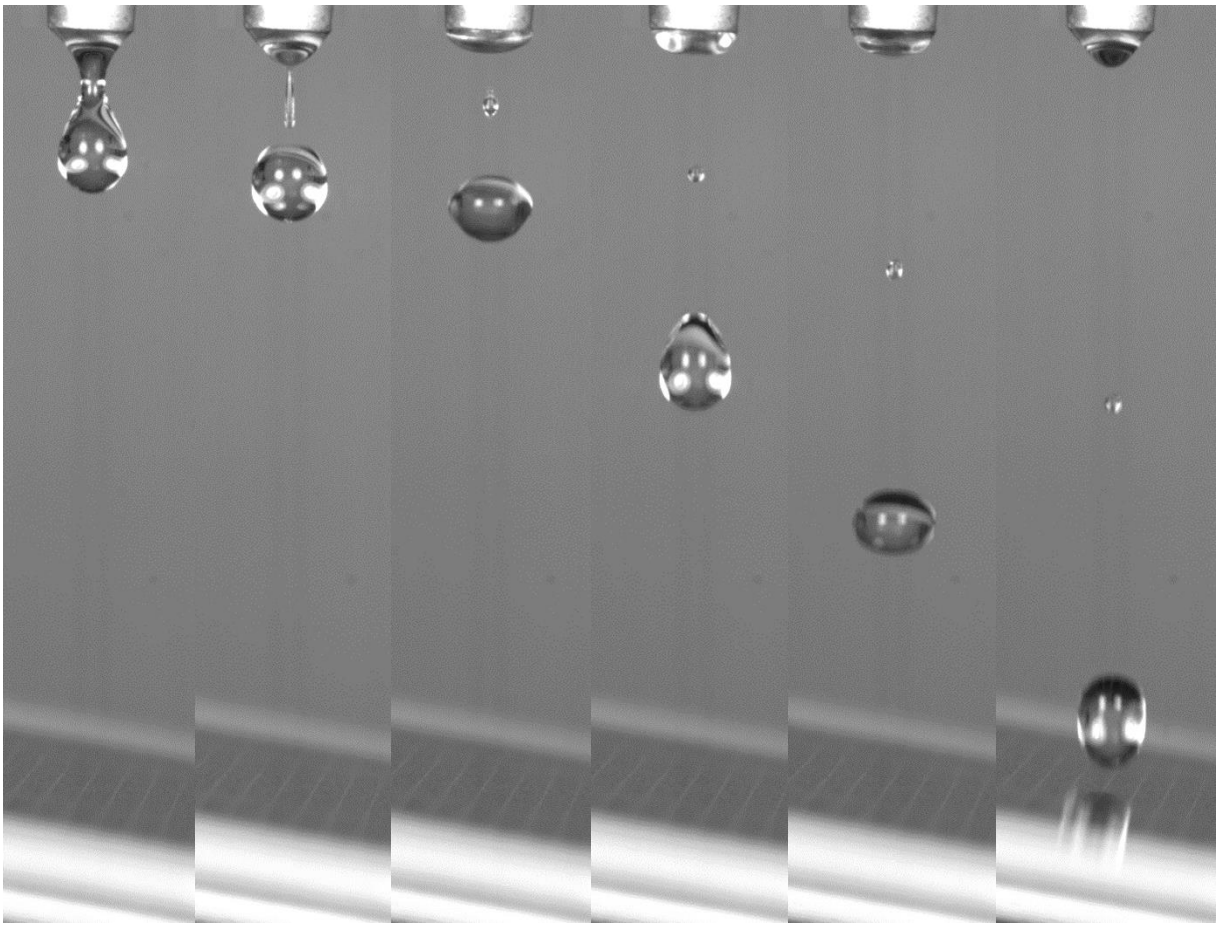

Figure 10. Oscillation observed in the falling drop resulting from release for Case 3.

Particle position tracking was used for velocity measurements. Figure 11 shows two time histories of particle velocity for Cases 9 and 10 that show some oscillation due to tracking a reflection on the surface that may shift as drop shape oscillates. These plots show the larger oscillations for the 1 m/s case as less time has elapsed since release for damping. To reduce the impact of shape oscillations affecting velocity measurements, the last five velocities were averaged. Again, Table 7 shows that, at least for the 3 m/s case, the repeatability for velocity was excellent. Future work may test the repeatability of the 1 m/s case that may be more susceptible.

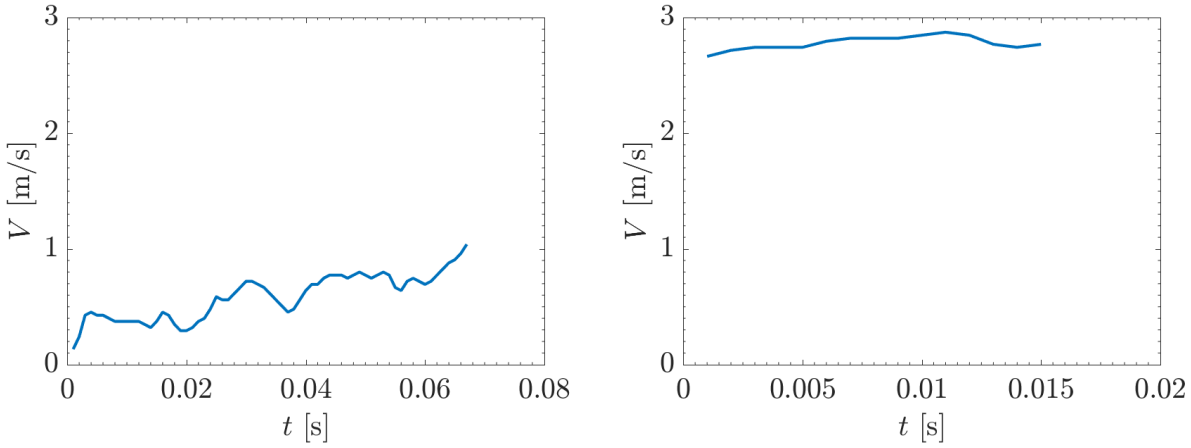

Figure 11. Velocity tracking as a function of time for the nominal 1 m/s Case 9 (left) and the nominal 3 m/s Case 10 (right).

4. CONCLUSIONS

In this study, both numerical models and tests of impinging water droplets on inclined glass surfaces were developed to investigate their behavior and potential for self-cleaning. A multiphase volume-of-fluid model was developed in ANSYS Fluent to simulate the impinging droplets. The simulations considered different droplet sizes (1 mm and 3 mm), tilt angles (0°, 10°, and 45°), droplet velocities (1 m/s and 3 m/s), and wetting characteristics (wetting=47° contact angle and non-wetting = 93° contact angle). Results showed that the spread factor (maximum droplet diameter during impact divided by the initial droplet diameter) decreased with increasing inclination angle due to the reduced normal force on the surface. The hydrophilic surface yielded greater spread factors than the hydrophobic surface in all cases. With regard to satellite droplet format following impact, the simulated results were similar for all cases at the same droplet velocity, although the lower 1 m/s velocity did not yield any satellite droplet formation. With regard to impact forces, the greater surface tilt angles yielded lower normal forces, but higher shear forces. It is not clear whether greater normal forces or shear forces will be more effective in the removal and uptake of particles/soiling during rainfall.

Experiments were also performed to investigate the physics of impinging droplets on inclined glass surfaces. Twelve cases were tested to investigate different wetting surfaces (hydrophilic vs. hydrophobic, surface tilt angle (0°, 10°, and 45°), and impact velocity (~1 m/s and ~3 m/s). Several of the cases were performed in triplicate and results showed that the tests were repeatable. Results showed that the experimentally observed spread factor (maximum droplet diameter during impact divided by the initial droplet diameter) was significantly larger than the simulated spread factor. Observed spread factors were on the order of 5 – 6 for droplet velocities of ~3 m/s, whereas the simulated spread factors were on the order of 2. The only observed satellite droplet formation occurred during the 45° tilt case with a ~3 m/s droplet velocity. Also, the droplets were mobile following impact only for the cases with 45° tilt angle, which matched the simulations. An interesting phenomenon that was observed was that shortly after being released from the nozzle, the water droplet oscillated (like a trampoline) due to the "snapback" caused by the surface tension of the water droplet being released from the nozzle. This oscillation impacted the velocity immediately after the release.

Future work should evaluate the impact of parameters such as tilt angle and surface wettability on the impact of particle/soiling uptake and removal to investigate ways that photovoltaic modules and heliostats can be designed to maximize self-cleaning.

REFERENCES

[1] Salim, A. A., Huraib, F. S., and Eugenio, N. N., "PV power-study of system options and optimization. In EC photovoltaic solar conference," 8, pp. 688-692, 1988.

[2] Hu, J., Bodard, N., Sari, O., and Riffat, S., "CFD simulation and validation of self-cleaning on solar panel surfaces with superhydrophilic coating," Future Cities and Environment, 1(1), 8, 2015.

[3] Quan, Y. Y., Zhang, L. Z., Qi, R. H., and Cai, R. R., "Self-cleaning of Surfaces: the Role of Surface Wettability and Dust Types," Scientific Reports, **6**, 2016.

[4] Fürstner, R., Barthlott, W., Neinhuis, C. and Walzel, P., 2005. Wetting and self-cleaning properties of artificial superhydrophobic surfaces. *Langmuir*, **21**, No. 3, pp.956-961, 2005.

[5] Burton, P. D., and King, B. H., "Spectral sensitivity of simulated photovoltaic module soiling for a variety of synthesized soil types," IEEE Journal of Photovoltaics, 4, No. 3, pp. 890-898, 2014.

[6] Aziz, S.D., Chandra, S., "Impact, recoil and splashing of molten metal droplets. International Communications in Heat and Mass Transfer," **43**, pp. 2841–2857, 2000.

[7] Link, K.C., Schlünder, E.-U., "Fluidized bed spray granulation. Investigation of the coating process on a single sphere. Chemical Engineering and Processing," **36**, pp. 443–457, 1997.

[8] Liu, H., "Science and Engineering of Droplets," Noyes Publications and William Andrew Publishing, LLC, Norwich, NY., 2000.

[9] Asai, A., Shioya, M., Hirasawa, J. and Okazaki, T., "Impact of an ink drop on paper," Journal of Imaging Science and Technology, 37, No. 2, pp. 205–207, 1993.

[10] Crooks, R., Cooper-White, J., Boger, D.V., "The role of dynamic surface tension and elasticity on the dynamics of drop impact," Chemical Engineering Science, **56**, No.19, pp.5575–5592, 2001.

[11] Pasandideh-Fard, M., Qiao, Y.M., Chandra, S., Mostaghimi, J., "Capillary effects during droplet impact on a solid surface," Physics of Fluids 8, 650–659, 1996.

[12] Werner, S.R., Jones, J.R., Paterson, A.H., Archer, R.H. and Pearce, D.L., "Droplet impact and spreading: Droplet formulation effects. Chemical Engineering Science," **62**, No. 9, pp.2336-2345, 2007.

[13] Hu, J., Bodard, N., Sari, O. and Riffat, S., 2015. CFD simulation and validation of self-cleaning on solar panel surfaces with superhydrophilic coating. Future Cities and Environment, **1**, No. 1, p.8, 2015.

[14] Lopez, J., Miller CA, Ruckenstein E, "Spreading kinetics of liquid drops on solids," J Colloid Interface Sci **53**, pp. 460–461, 1976.

[15] Yeo, L., "Wetting and Spreading, Encyclopedia of Microfluidics and Nanofluidics," pp 2186–2196, 2008.

[16] Kavehpour HP, Ovryn B, McKinley GH, "Evaporatively-driven Marangoni instabilities of volatile liquid films spreading on thermally conductive substrates," Coll Surf A, **206**, pp. 409–423, 2002.

[17] Oron A, Davis SH, Bankoff SG (1997) Long-scale evolution of thin liquid films. Rev Mod Phys 69(3):931.

[18] Bonn D, Indekeu J, Meunier J, Rolley E, "Reviews of Modern Physics," **81**, pp.739–805, 2009.

[19] Scheller, B.L., Bousfield, D.W., "Newtonian drop impact with a solid surface," A.I.Ch.E. Journal 41 (6), 1357–1367, 1995.

[20] Biance A-L, Clanet C, Quere D, "First steps in the spreading of a liquid droplet," Phys Rev E, **69**, 2004.

[21] Bird JC, Mandre S, Stone HA, "Short-time dynamic of partial wetting," Phys. Rev. Lett. 100, 2008.

[22] Jepsen, R.A. and Brown, A., "Extreme Impact Events for Glycerin Provide new Insights for Splash Dynamics," (No. SAND2009-1156C). Sandia National Laboratories (SNL-NM), Albuquerque, NM (United States), 2009

[23] Yoon, S.S., Jepsen, R.A., Nissen, M.R., O'Hern, T.J., "Experimental investigation on splashing and nonlinear fingerlike instability of large water drops," Journal of Fluids and Structures, 23:101-115 (2007).

[24] Brown, A.L., Jepsen, R.A., and Yoon, S.S., "Modeling Large-scale Drop Impact: Splash Criteria and Droplet Distribution," ILASS Americas, 21st Annual conference on Liquid Atomization and Spray Systems, Orlando, FL, May 18-21, 2008.

[25] Cossali, G.E., M. Marengo, and M. Santini, "Single-Drop Empirical Models for Spray Impact on Solid Walls: A Review," Atomization and Sprays, **15**, pp. 699-736, 2005.

[26] Brown, A.L. and Jepsen, R.A., "Drop Fingering on Oblique Impact: Part 2—Modeling," ICLASS, 2009.

[27] Yarin, A.L., "Drop Impact Dynamics: Splashing, Spreading, Receding, Bouncing…," Annu. Rev. Fluid Mech. **38**, pp. 159-192, 2006.

[28] Leneweit, G., R. Koehler, K.G. Roesner, and G. Schafer, "Regimes of drop morphology in oblique impact on deep fluids," J. Fluid Mech., 543, 303-331, 2005.

[29] Okawa, T., T. Shiraishi, and T. Mori, "Effect of impingement angle on the outcome of single water drop impact onto a plane water surface," Exp. Fluids 44:331-339, 2008.

[30] Jepsen, R.A., Yoon, SS, Demosthenous, B., "Effects of Air on Splashing during a Large Droplet Impact," Atomization and Sprays, 16, 1-16, 2006.

[31] Jepsen, R.A., Brown, A., Aguilar, G. and Vu, H., 2009. Drop Fingering on Oblique Impact: Part 1--Experimental Data (No. SAND2009-0496C). Sandia National Laboratories (SNL-NM), Albuquerque, NM (United States).

[32] J. E. Field, M. B. Lesser, and J. P. Dear, "Studies of two-dimension liquid-wedge impact and their relevance to liquid drop impact problems," Proc. R. Soc. London, Ser. A 401, 225–249, 1985.

[33] J. P. Dear and J. E. Field, "High speed photography of surface geometry effects in liquid/solid impact," J. Appl. Phys. **63**, pp. 1015–1021, 1988.

[34] J. E. Field, J. P. Dear, and J. E. Ogren, "The effect of target compliance on liquid drop impact," J. Appl. Phys. **65**, pp. 533–540, 1989.

[35] F. J. Heymann, "High speed impact between a liquid drop and a solid surface," J. Appl. Phys. **40**, pp. 5113–5122, 1969.

[36] W. F. Adler, "Water Impact Modelling," Wear, **186**, pp. 341–351, 1995.

[37] Y. C. Huang, F. G. Hammitt, and W. J. Yang, "Hydrodynamic phenomena during high-speed collision between liquid droplet and rigid plate," J. Fluids Eng. **95**, pp. 276–292, 1973.

[38] M. H. Keegan, D. H. Nash, and M. M. Stack, in Proceedings of the ASME Turbo Expo 2012: Turbine Technical Conference and Exposition, Copenhagen, Denmark, 11 June-15 June 2012 (American Society of Mechanical Engineers, New York, 2012), pp. 887–898, 2012.

[39] N. Li, Q. L. Zhou, X. Chen, T. M. Xu, S. E. Hui, and D. Zhang, "Liquid drop impact on solid surface with application to water drop erosion on turbine blades, Part I: Nonlinear wave model and solution of one-dimensional impact," Int. J. Mech. Sci. **50**, pp. 1526–1542, 2008.

[40] Q. L. Zhou, N. Li, X. Chen, T. M. Xu, S. E. Hui, and D. Zhang, "Liquid drop impact on solid surface with application to water drop erosion on turbine blades, Part II: Axisymmetric solution and erosion analysis," Int. J. Mech. Sci. **50**, pp. 1543–1558, 2008.

[41] Li, J., Zhang, B., Guo, P. and Lv, Q., "Impact force of a low speed water droplet colliding on a solid surface. Journal of Applied Physics," **116**, No. 21, 2014.

[42] Gupta, V.K., Khan, M. and Punekar, H., "Development and Application of Interfacial Anti-Diffusion and Poor Mesh Numerics Treatments for Free Surface Flows," High Performance Computing Workshops (HiPCW), 2015 IEEE 22nd International Conference on (pp. 12-18). IEEE, 2015.

[43] Ansys, A.F., "14.0 Theory Guide," ANSYS inc, pp.218-221, 2011.

[44] Liu, J., Vu, H., Yoon, S.S., Jepsen, R.A. and Aguilar, G., 2010. Splashing phenomena during liquid droplet impact. Atomization and Sprays, **20**, No. 4, 2010.

[45] Linstrom, P.J. and Mallard, W.G., 2001. "NIST Chemistry webbook," NIST standard reference database No. 69.

[46] Brackbill, J.U., Kothe, D.B. and Zemach, C., "A continuum method for modeling surface tension. Journal of computational physics," **100**, No.2, pp.335-354, 1992.

DISTRIBUTION

All Electronic

1	MS0899	Technical Library	9536
1	MS0359	D. Chavez, LDRD Office	1911


Sandia National Laboratories